Dissecting the geometric and hydrophobic constraints of stapled peptides

(Running title: Action mechanism of stapled peptides)

Jianguo Li[1,2,*], Yaw Sing Tan[1], Chandra Verma[1,3,4,*]

[1]Bioinformatics Institute, Agency for Science, Technology and Research (A*STAR), 30 Biopolis Street, #07-01 Matrix, Singapore, 138671

[2]Singapore Eye Research Institute, Singapore, 169856, Singapore.

[3]National University of Singapore, Department of Biological Sciences, Singapore.

[4]Nanyang Technological University, School of Biological Sciences, Singapore.

*Corresponding author:
lijg@bii.a-star.edu.sg
chandra@bii.a-star.edu.sg

Abstract: Stapled peptides are a promising class of molecules with potential as highly specific probes of protein-protein interactions and as therapeutics. Hydrocarbon stapling affects the peptide properties through the interplay of two factors: enhancing the overall hydrophobicity and constraining the conformational flexibility. By constructing a series of virtual peptides, we study the role of each factor in modulating the structural properties of a hydrocarbon stapled peptide PM2 which has been shown to enter cells, engage its target MDM2 and activate p53. Hamiltonian replica exchange molecular dynamics (HREMD) simulations suggest that hydrocarbon stapling favors helical populations of PM2 through a combination of the geometric constraints and the enhanced hydrophobicity of the peptide. To further understand the conformational landscape of the stapled peptides along the binding pathway, we performed HREMD simulations by restraining the peptide at different distances from MDM2. When the peptide approaches MDM2, the binding pocket undergoes dehydration which appears to be greater in the presence of the stapled peptide compared to the linear peptide. In the binding pocket, the helicity of the stapled peptide is increased due to the favorable interactions between the peptide residues as well as the staple and the micro-environment of the binding pocket, contributing to enhanced affinity. The dissection of the multi-faceted mechanism of hydrocarbon stapling into individual factors not only deepens fundamental understanding of peptide stapling, but also provides guidelines for the design of new stapled peptides.

1. Introduction:

Peptides are a promising class of molecules that can serve as probes of molecular interactions as well as therapeutics[1, 2]. In contrast to small-molecule drugs, they can bind to protein-protein interfaces, especially those that are flat and hence not amenable to binding small molecules. In addition, their large size enables them to engage more extensive surfaces, thus endowing them with high specificity, characteristics that are lacking in small molecules. Their smaller size compared to biologics (antibodies) gives them the advantage of entering cells, enabling them to target intracellular pathways. However, peptide drugs also have several disadvantages that limit their clinical applications: (a) they are prone to proteolytic digestion, resulting in low stability; (b) they are flexible and adopt an ensemble of diverse conformations in solution that results in reduced affinities for their receptors (this is largely due to the entropic cost of undergoing a conformational change from extended to folded conformations upon binding); (c) they are mostly not cell-permeable because of their polar nature. Several of these limitations can be overcome by chemical modifications of the peptide backbone and sidechains, such as macrocyclization, the use of D-amino acids and incorporation of unnatural amino acids [3]. Among these modifications, peptide stapling, in which the side chains of a pair of residues are covalently connected by a staple chain, has been demonstrated to confer desirable properties [4-11]. Incorporation of the staple chain restricts the diversity of peptide conformations, and when rationally placed to mimic the bound state conformation, results in a reduction in the entropic penalty upon binding. Indeed, a recent study showed that the lower entropic penalty in the unbound state is the major contributor to the improvement of binding affinity of stapled peptides[12, 13]. Although non-covalent stapled peptides based on Glu-Lys salt bridges can also stabilize the peptide conformation, the non-covalent linkage is not stable and the charged residues may incur high free energy barriers during membrane penetration[14-17]. Covalent stapling has been shown to increase the therapeutic properties of peptides[6, 7, 18-24]. The presence of covalent staples not only shields the backbone atoms thus making the peptides resistant to proteolysis[18, 25, 26], but also favors cell penetration[27, 28] The Verdine/Walensky groups from Harvard pioneered the use of stapled peptides in biology and has designed a number of stapled and stitched peptides targeting various pathways with enhanced cell penetration[29-32] including activating p53 in oncology, inhibiting viral fusion and targeting bacterial membranes[33-36]. These efforts have greatly accelerated the clinical development of stapled peptide therapeutics and a peptide that came out of the efforts of the Verdine group spinoff Aileron Therapeutics. ALRN-6924, has recently entered clinical trials[37]. Several other groups such as that of Grossman, David Spring, etc have expanded the space of stapling as well as the targets [38-40]. Of the several strategies adopted to develop stapled peptides [41], a commonly used one is to connect two positions along the peptide sequence with an alkyl chain. The advantage of hydrocarbon stapling is that the staple chain shields the intervening backbone atoms from water and enhances the overall hydrophobicity of the

peptide, resulting in enhanced membrane permeability[18, 25, 42]. Despite the advantageous properties of hydrocarbon stapling, and several reports of their successful deployment for inhibiting a variety of protein-protein interactions, the details of the associated mechanisms remain poorly understood, limiting rigorous rational development. These issues are being explored by research groups combining biophysical experiments such as X-ray and NMR along with molecular dynamics (MD) simulations [43, 44].

Several stapled peptides have been developed to inhibit the interactions between the tumor suppressor protein p53 and its negative regulator protein the Mouse Double Minute 2 (MDM2). These peptides have been designed to mimic the N-terminal region of p53 that binds to the N-terminal region of Mdm2, inhibit the latter and release p53 to carry out its biological functions [45 4, 5, 18, 46, 47]; one such peptide is also in clinical trials [37]. Combinations of various experimental techniques with computer simulations have provided a wealth of atomistic insights into the mechanisms characterizing these peptides. A major area of enquiry has focused on the solution behavior of these stapled peptides. Guo et al have explored a set of such p53 mimicking, MDM2 binding peptides using MD simulations[48] and found that stapling stabilizes the helicity of these peptides; unsurprisingly, the helicity varied depending on the peptide sequence as well as on the staple positions. Joseph et al were the first to explore, through MD simulations, the interactions of the p53 mimicking unstapled and stapled peptides with MDM2[49]. They found that in addition to increased helicity, higher affinity appeared to result from a significant contribution of engagement between the staple and the surface of MDM2. This interaction was subsequently confirmed by crystallographic studies[32]. Sim et al. compared the atomistic details of the binding of unstapled and stapled peptides to MDM2 and found that the stapled peptides have a higher tendency to bind to the pocket of MDM2 than the unstapled ones, driven by a deeper free energy funnel [43].

Several studies have subsequently explored the free energies of binding of stapled peptides[50, 51]. Although the computation of the binding free energies for small molecule ligands is straight forward and well established, for peptides such calculations often suffer from convergence problems arising from insufficient sampling [52]. Guo et al. used umbrella sampling to compute the binding free energy of several stapled peptides, but the results were found to be dependent on the binding pathway, highlighting the sampling challenges faced in the computational predictions of the binding free energies of stapled peptides. In contrast, the computation of relative binding free energies of peptides with respect to that of a reference peptide appears to be more reliable[50]. Morrone et al. used the MELD (Modeling by Employing Limited Data) method to calculate the relative binding affinities of a series of stapled peptides for MDM2[51]. Their method not only identified the right binding pose, but also predicted binding affinities consistent with experiments. The interactions between the N-terminal regions of p53 and MDM2 were found to be driven by evolutionarily conserved residues[53]. Furthermore, the mechanism

and role of the displacement of waters that solvate the p53 binding pocket of MDM2 was explored by Sim et al [42] who found that the stapled chain "induces" dewetting of the surface of the binding pocket, a behavior seen during the association of large hydrophobic interfaces[42, 54], suggesting that the dehydration of the binding pocket is enthalpically driven. Subsequently, Lee et al.[55] found that not all the water molecules associated with the p53 binding pocket are excluded during binding. They identified one to two water molecules that appear to assist peptide binding by forming hydrogen bonds that bridge Tyr99 of MDM2 and the backbone of the C-terminal region of the stapled peptide. Indeed, Guo et al.[50] found more than 100 hydration sites on the surface of the binding pocket of MDM2 and although most of these water molecules displayed dynamic behavior similar to that of bulk water, several water clusters were thermodynamically unstable and their release to bulk water during peptide binding were hypothesized to significantly improve the free energy of binding.

The above studies provided valuable information for understanding the role of hydrocarbon stapling in modulating the solution helicity and binding mechanisms of the stapled peptide, but a rigorous understanding of the individual physical factors of hydrocarbon stapling is still lacking. It is clear that hydrocarbon stapling modulates the peptide conformation via some interplay between the geometric constraints imposed by the act of stapling (referred as the constraint effect hereafter) and the enhanced peptide hydrophobicity due to the hydrocarbon chain (referred as the hydrophobic effect hereafter); however, their individual contributions in modulating the peptide helicity are not clear. Insights into the two effects could be useful in optimizing the length and chemistry of the staple chain. Moreover, the peptide conformation strongly depends on the micro-environment [56]. As the peptide approaches the binding pocket from the bulk aqueous phase, the peptide will experience some conformational adaptations in response to changes in the micro-environment (partitioning from bulk phase to a semi buried state upon being embedded in the target, which is MDM2 in the current study). Although several studies have focused on the peptide conformation in the binding pocket [43, 50], the conformational changes along the binding pathway have not been characterized in detail.

In this study, we employ rigorous MD simulations to dissect the effects that hydrophobicity and geometric constraints of hydrocarbon stapling have on the internal dynamics of the peptide and its interactions with its target. We explore these effects using a stapled peptide called PM2 which has been demonstrated to enter cells, bind its target MDM2 with high affinity and result in p53 activation[57, 58]. The MDM2-PM2 complex represents a good model to study the role of hydrocarbon stapling because X-ray structures of MDM2 complexed with a PM2 variant [58] and an unstapled counterpart [59] are available and it has been well-characterized using experimental and computational methods[58, 60, 61]. We used replica exchange with solute tempering (REST) simulations[62, 63], also known as Hamiltonian replica exchange molecular dynamics (HREMD)

simulations[64, 65] to examine the constraint effect and the hydrophobic effect of hydrocarbon stapling separately using PM2 and another 3 virtual peptides (Figure 1). In the first peptide (referred to as PM2-spring), we replaced the hydrocarbon staple by a harmonic spring, thus eliminating the hydrophobic effect and retaining only the constraint effect. To understand how the hydrophobicity of the staple chain modulates the peptide conformation, in the second peptide (referred to as PM2-PEG), we modified the hydrocarbon chain into a hydrophilic polyethylene glycol (PEG) chain consisting of three ethylene glycol units. We chose three ethylene glycol units so to ensure that the ensuing chain length is the same as that of the hydrocarbon staple chain. Therefore PM2-PEG has reduced hydrophobicity while still retains the geometric constraint. The third peptide (referred to as PM2-linear) is an unstapled peptide (the stapling sites along the peptide chain are mutated into Ala), where both the constraint and the hydrophobic effects are eliminated. We also carried out HREMD simulations to explore how hydrocarbon stapling modulates the conformations of the peptides and associated free energy landscapes in detail as they approach the binding pocket in MDM2. We find that hydrocarbon stapling modulates the conformational landscape of PM2 in solution. This manifests in enhancing its affinity for its receptor MDM2 through two effects: attenuation of the entropic penalty that results from constraining the peptide to its bound conformation and contacts that hydrocarbon chain makes with the surface residues of MDM2, in agreement with previous studies[32]. We also discussed the effect of stapling on the chemical equilibrium of binding, e.g., how stapling changes the binding mechanism from a two-equilibrium process to a one-equilibrium process.

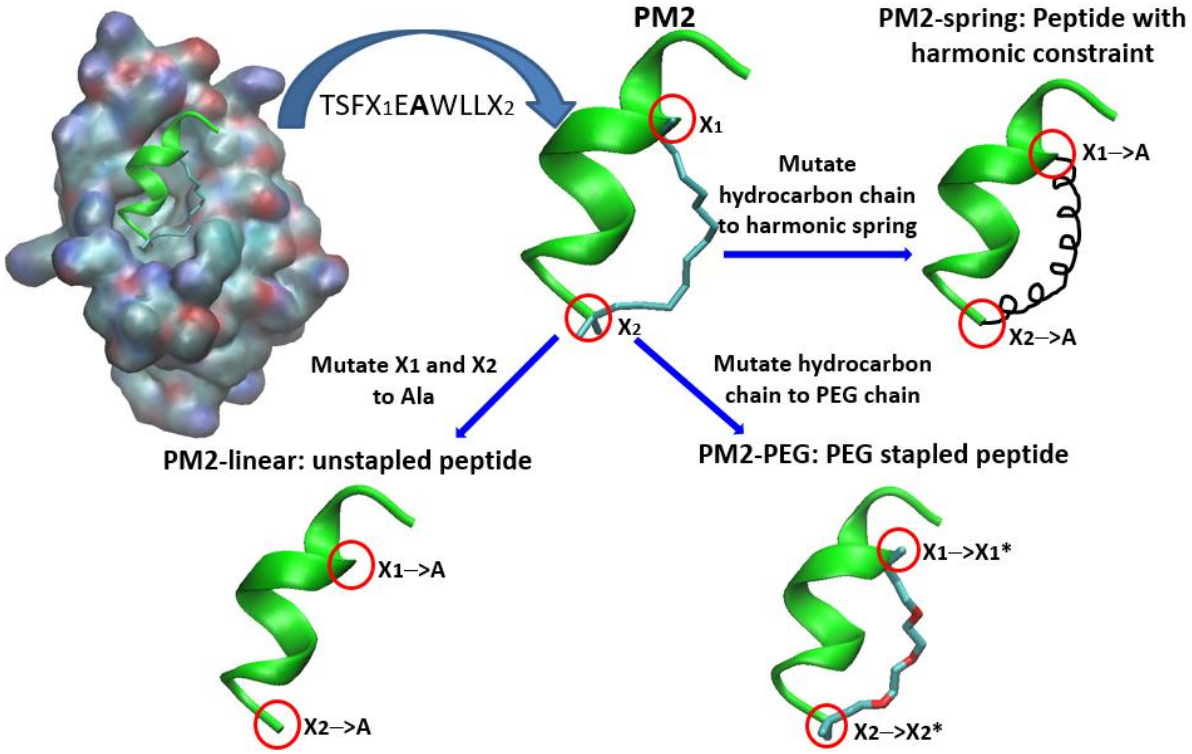

Figure 1. In silico construction of the peptides used in HREMD simulations. PM2 is derived using the stapled peptide in the PDB file 4UMN (MDM2 is shown as surface on the left and is complexed to the peptide in green with sequence $TSFX_1EYWYLLX_2$; the staple chain is shown as sticks and residues X_1 and X_2 are stapling sites) which is changed to PM2 by mutating the Tyr at position 8 to Ala (shown in bold in the sequence in the figure). The PM2-linear peptide is generated by mutating X_1 and X_2 to Ala. The PM2-spring peptide is constructed by mutating X_1 and X_2 to Ala and the hydrocarbon chain to a harmonic spring. The PM2-PEG stapled peptide is constructed by mutating X_1 and X_2 to X_{1*} and X_{2*} and connecting the two side chains, in which the hydrocarbon staple chain is replaced by 3 PEG units.

2. Methods:

The crystal structure of MDM2 complexed with a stapled peptide with sequence Ac-$TSFX_1EYWYLLX_2$-NH_2 (where X_1 and X_2 indicate the stapling sites; PDB code 4UMN, resolved at 0.2 nm [58], and Ac and NH2 refer to the acetyl and amide groups that are used to cap the N and C termini respectively) was used for our studies. The PM2 molecule was created by mutating the residue Y8 to alanine[58]. We explore the conformational dynamics of PM2, its unstapled analogue with alanine at the stapling positions 4 & 11 (referred to as PM2-linear), a peptide in which the staple chain is replaced by a harmonic spring (referred as PM2-spring) and a fourth peptide in which the hydrocarbon chain is mutated into a hydrophilic chain consisting of three PEG monomers with length similar to that of the hydrocarbon chain in the staple (referred to as PM2-PEG) (Table S1 and Figure 1), using HREMD simulations [63, 64, 66, 67]. In each HREMD simulation, 8 replicas with different Hamiltonians were simulated in parallel. The solute-solute and solute-solvent interactions were rescaled from 100% of the original interactions for the first replica to a certain percentage (usually 50%) for the last replica, while the solvent-solvent interactions were retained as normal. At certain time intervals, a Monte Carlo move was attempted to exchange the conformations of adjacent replicas with the acceptance governed by the Metropolis criterion[68]. This ensures that the system is not stuck in any local minimum of the free energy surface and instead can efficiently sample the phase space[69]. To obtain unstructured conformations of the peptides in solution to initiate the HREMD simulations, we performed a short MD simulation performed on the folded structures of PM2 and PM2-PEG, with the interactions involving the peptide atoms rescaled to 50%. This resulted in their unfolding (A high temperature was also used for PM2-PEG to accelerate unfolding). The unfolded state of PM2 was used to generate PM2-linear and PM2-spring by mutating the residues at the stapling sites of PM2 into alanine. Next, each of the 4 unfolded states (Figure S1) was subject to HREMD simulations for 200 ns. Analysis of the trajectories was carried out over the last 100 ns.

To understand how hydrocarbon stapling modulates the binding mechanism of PM2, HREMD simulations were also performed on PM2, PM2-linear, PM2-PEG and PM2-

spring, in complex with MDM2, respectively. The initial conformation of the complex of PM2 with MDM2 was taken from a crystal structure (PDB ID 4UMN, resolution: 0.2 nm)[58], while the complex of the other three peptides with MDM2 was constructed by mutating PM2 bound to MDM2. In addition to the simulations where each peptide was in the binding pocket, a series of HREMD simulations were also carried out with the peptides placed at increasing distances from MDM2. The distance between the center of mass of the folded peptide and the center of mass of MDM2 was set at 1.4, 1.7 and 2.1 nm and at each distance, a harmonic potential with a force constant of 1000 kJ mol^{-1} nm^{-2} was added to the center of mass of the peptide with respect to the center of mass of MDM2 to maintain the distance. (Figure S1); The distances were chosen because at 1.4 nm the peptide is displaced from its bound state, but still within the binding pocket; at 1.7 nm the peptide is further displaced away from the bound state while at 2.1 nm, it is completely out of the binding pocket. The aim is to understand the conformational changes associated with the peptide as it approaches the binding pocket. The alpha-carbon atoms of MDM2 were position restrained so that the binding pocket remains open during the HREMD simulation. In each HREMD simulation, 8 replicas were used with the non-bonded interactions and the dihedral potentials involving the peptide atoms gradually rescaled from 100% to 50%, while keeping other interactions unchanged. In particular, the LJ potentials were rescaled by adjusting the parameter epsilon, while the electrostatic potentials were rescaled by adjusting the partial charges of each atom. The dihedral potentials were rescaled by adjusting the force constant.

All the simulations were carried out using the AMBER99sb force field [70] coupled with the TIP3P water model [71]. We chose this combination as it has been extensively benchmarked by several groups including ours, producing models that are consistent with experimental data[43, 72-75]; there are reports that suggest that AMBER14sb showed improved accuracy over AMBER99sb in certain systems, but for the MDM2-p53 complex, both force fields have been shown to give similar results[76, 77]. The parameters of the unnatural amino acids at the staple sites of PM2 were obtained from previous studies [43, 49, 73], while the parameters of the PEG chain were obtained using antechamber[78]. In the peptide PM2-spring, a harmonic spring with the force constant of 500 kJ/mol/nm^2 was applied to restrain the distance between the alpha carbon atoms of residue 5 and residue 12 to be 1.12 nm, which corresponds to the distance when the peptide is in helical conformation. Counter ions were added to neutralize the simulation box. Short-range electrostatic interactions and van der Waals interactions were calculated by a cut-off scheme of 1.0 nm, while long-range electrostatic interactions were computed using PME[79]. The details of all the simulated systems were included in Table S2. We found 8 replicas result in sufficient overlap in the potential energy distribution between adjacent replicas and can achieve an average acceptance ratio between 20%-35% (Figure S2). All the simulations were performed in the NPT ensemble with the temperature and pressure maintained at 300K and 1 bar using Nose-Hoover thermostat and Parrinello-Rahman

barostat, respectively. The Links algorithm was applied which enables a time step of 2 fs during the MD simulations. The simulations of the peptides in solution were run for 200 ns, and the simulations of the complex were run for 300 ns. In each simulation, the first 100 ns was discarded, and the analysis was performed for the rest of the trajectory. The secondary structure evolution during the simulations was calculated using DSSP[80]. The water density around the binding pocket of MDM2 was calculated using the grid module of the AMBER20 package[81]. Binding energies were calculated using g_mmpbsa. This method calculates two energies: the change of gas state energy upon binding ΔE_{gas} (e.g., direct interaction energy without including solvent) and the change of solvation energy upon binding, ΔG_{solv} (corresponding to the energy of transferring a molecule from gas state to solvent). The change of gas state energy ΔE_{gas} is the sum of vdw (ΔE_{vdw}) and electrostatic contributions (ΔE_{ele}), while the change of solvation energy ΔG_{solv} is the sum of polar solvation energy ($\Delta G_{solv,polar}$) and the non-polar solvation energy ($\Delta G_{solv,non\text{-}polar}$). The polar solvation energy is calculated by solving the Poisson-Boltzmann equation and is highly positive in typical MMPBSA calculations, reflecting the change of electrostatic interactions between the solute and the solvent upon binding[82, 83]. In addition, the sum of $\Delta G_{solv,polar}$ and ΔE_{ele} gives an estimate of the penalty that is paid for the protein and peptide to form a complex as both move partially out of bulk solvent. All simulations were performed using the GROMACS 4.6 package patched with PLUMED[84, 85].

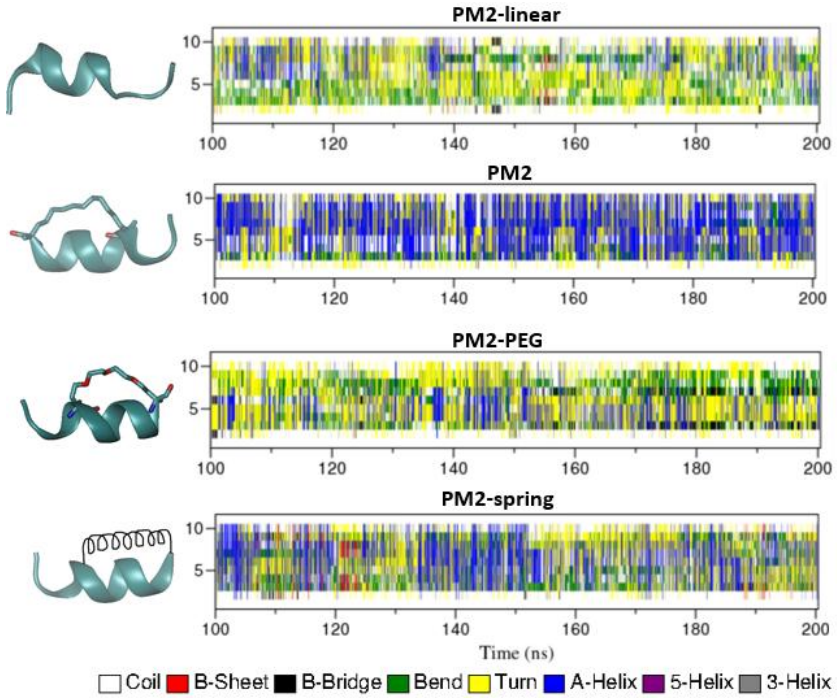

Figure 2. Secondary structural changes of the different peptides in solution during the last 100 ns of HREMD simulations. Y-axis is the residue index.

3. Results

3.1 Hydrocarbon stapling favors helical conformation in solution

The introduction of a hydrocarbon staple can affect the peptide conformation by acting as a distance constraint that restricts the peptide from adopting extended conformations and by providing a hydrophobic environment to stabilize nonpolar side chains and partially shield the polar backbone from attack by water molecules; this may promote helical conformations. To distill out these possibilities, we carried out HREMD simulations on a stapled peptide PM2 and three variants including an unstapled peptide (PM2-linear), a peptide with its staple replaced by a virtual harmonic spring (PM2-spring) and a variant where PEG replaces the hydrocarbon staple (PM2-PEG). The evolution of the secondary structures during the simulations (Figure 2 and Table S3) reveals that along with different degrees of alpha-helicity, the peptides also adopt certain populations of 3-10 helical conformations. It is clear that PM2 displays the highest degree of helicity followed by PM2-spring, PM2-PEG and the unstapled peptide PM2-linear. PM2-spring is more helical than PM2-linear, suggesting that the constraint effect itself partially accounts for the enhanced helicity of the stapled peptide. Interestingly, although PM2-spring has lower alpha-helicity compared to PM2, it displays a higher percentage of 3-10 helicity. The overall helicity for PM2-spring (the sum of alpha-helix and 3-10 helix) is 30.9% (Table S3), which is much higher than for the unstapled PM2-linear. Compared to the alpha-helix in which hydrogen bonds formed between residues (i, i+4), the hydrogen bonds in 3-10 helix are formed between residues (i, i+3). Hence 3-10 helix is thinner and the backbone atoms are more exposed to water molecules. Studies also showed that 3-10 helix usually appears at N and C terminal regions of a peptide or in short peptides, suggesting a correlation between the population of 3-10 helix and the backbone hydration[86, 87]. In PM2-spring, the lack of staple chain to stabilize the hydrophobic side chains results in higher 3-10 helix population. As a result, the PM2-spring displays higher backbone hydration. Therefore the 3-10 helix appears to be localized largely to the exposed N or C termini[88]. The absence of the hydrocarbon staple chain in PM2-spring results in reduced sidechain packing (compared to PM2), and this allows for higher backbone hydration, resulting in higher 3-10 helix population. Moreover, for some short peptides, 3-10 helices have been shown to be thermodynamically inter-changeable with alpha-helices, with only ~2kJ/mol free energy difference between the two states[89, 90]. In contrast, the introduction of polar atoms in the staple chain destabilizes the helical conformation of the peptide. When the hydrocarbon staple chain is replaced by a polar PEG chain, the helicity is significantly reduced, suggesting that hydrophobicity is critical in stabilizing the helical conformations of PM2. This may arise from the hydrophobic associations of the hydrocarbon chain with the hydrophobic residues of PM2 such as Phe and Trp; and this sidechain packing shields the peptide backbone from the water molecules, thus stabilizing the main-chain hydrogen bonds that favor the helical conformation. Nevertheless, because of the constraint effect, the PM2-PEG peptide has slightly higher overall helicity (17%) than the PM2-linear peptide (13.8%), as a result of a higher degree of 3-10 helical conformations. Together,

these observations suggest that the constraint effect appears to favor 3-10 helices while the hydrophobic hydrocarbon chain shifts the 3-10 helical states towards alpha-helical states. We also bin the peptide conformations into different clusters based on a RMSD cutoff value of 0.2 nm. Figure S3 shows snapshots of the peptide conformations representative of the three largest clusters. The largest cluster of PM2 displays a helical conformation and occupies 29% of the conformational space, while the population of the largest cluster for PM2-linear is 2.6% and only partially helical, suggesting that the unstapled peptide PM2-linear is highly dynamic in solution. The largest clusters for the other two peptides (PM2-PEG and PM2-spring) are also partially helical and show intermediate populations, consistent with the secondary structure results in Figure 2. Once again, it is clear that hydrocarbon stapling reduces the conformational flexibility of the peptide and shifts the phase space of the peptide towards helical conformations.

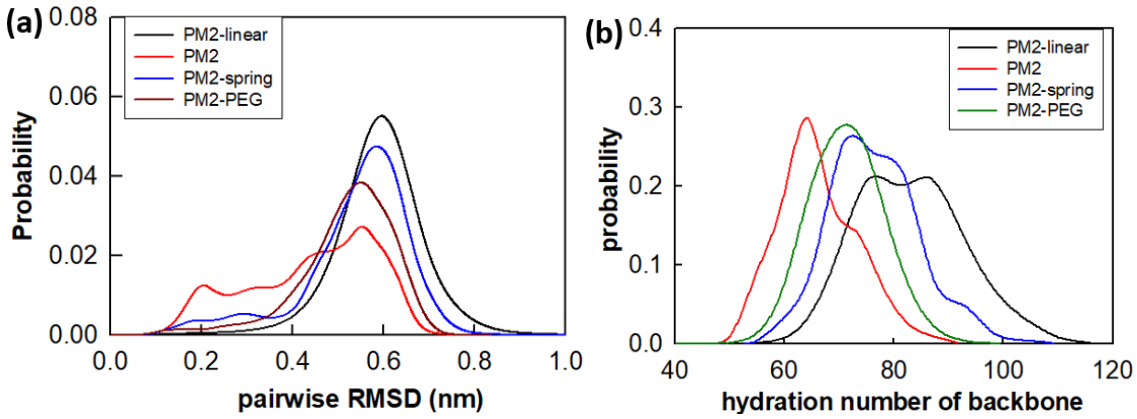

Figure 3. (a) Pair-wise RMSD of the four peptides in solution; (b) The probability distributions of the hydration number of backbone atoms of the 4 peptides in the solution. Water molecules within 0.5 nm of peptide molecule are defined as hydration water. The calculations is based on the last 100ns of the simulations.

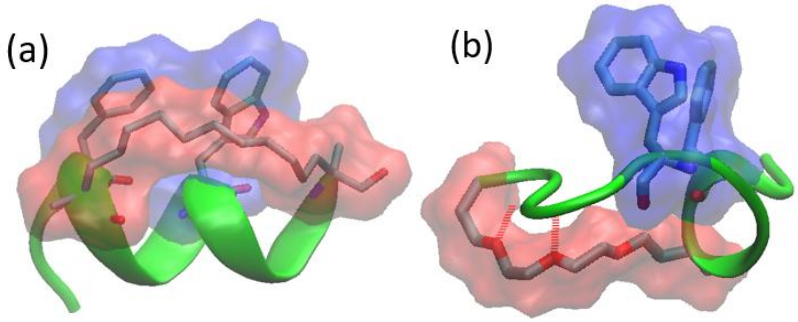

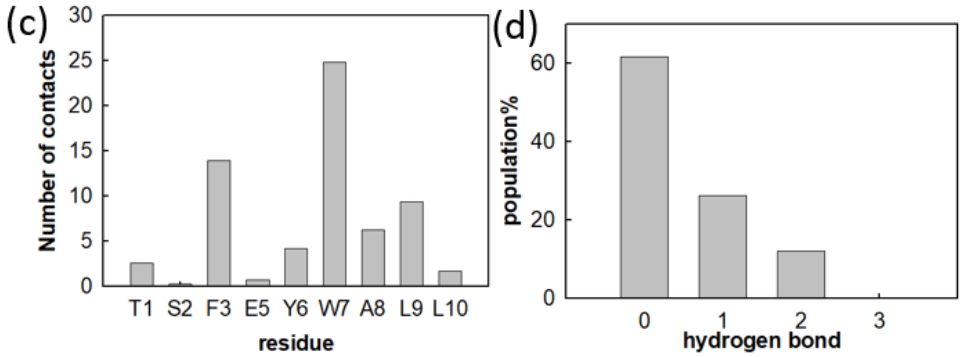

Figure 4. (a) Snapshot of PM2; (b) Snapshot of PM2-PEG showing two hydrogen bonds (red dashed lines) between the PEG chain and the backbone; (c) number of contacts between the hydrocarbon chain with the side chains of each residue; and (d) the number of hydrogen bonds between the PEG chain and the backbone. In Figures (a) and (b), TRP and PHE residues are represented by licorice and transparent surface (blue), the staple chain is represented by licorice and transparent surface (red).

To further understand the conformational flexibility of the four peptides, we calculated the pairwise RMSD between the conformations sampled by each peptide (over the last 100 ns of each trajectory (Figure 3a). Unlike proteins, peptides are small and the side chain orientation can significantly affect the RMSD, therefore we used all the peptide atoms to calculate RMSD. The pairwise RMSD is defined as the RMSD of each conformation sampled relative to every other conformation sampled (this characterizes the flexibility of the peptides) and has been shown to be related to the B-factor [91]. The results reveal that the unstapled peptide PM2-linear adopts the most diverse conformations while PM2 is the most restrained, and the other two peptides are characterized by intermediate flexibilities, as we have seen above. Hence, there is a clear correlation between peptide flexibility and helicity. We also performed PCA analysis of the four peptides using the last 100 ns of the trajectory. Figure S4 plots the free energy landscapes of the peptides using the first and second principal components (PC1 and PC2) as the reaction coordinates. The unstapled peptide PM2-linear is characterized by a rough free energy surface consistent with its high flexibility while the others show deep minima.

Although all the three peptides with constraints (e.g, PM2, PM2-spring and PM2-PEG) display higher helicity than the unstapled peptide, the helicity of PM2 is much higher than the two virtual peptides, suggesting the hydrophobicity of the staple chain also plays an important role. It appears that the hydrocarbon staple nucleates the formation of a hydrophobic cluster between the hydrocarbon staple and the side chains of F3 and W7 (Figures 4a 4c), stabilized by the associated reduction in the solvation free energy of both the hydrocarbon staple chain and the hydrophobic moieties. The backbone atoms beneath the staple largely remained shielded from the solvent, and in the absence of approach by water molecules, tend to form intra-molecular hydrogen bonds, thus favoring helical conformations. The importance of a hydrophobic environment in promoting helix

formation has been known[56, 92]. For example, trifluoroethanol (TFE) is known to induce helical conformations in peptides because the trifluoromethyl group of TFE faces and stabilizes the hydrophobic residues, while the hydroxyl group faces the solvent water, stabilizing the hydrophobic residues in helical conformation[93]. In the case of PM2-PEG, the polar oxygen atoms of the PEG units interact with water molecules as well as the polar atoms of the peptide backbone, thus disrupting the stability of the backbone hydrogen bonds. The number of water molecules within 0.5 nm of the backbone atoms calculated from the last 100 ns of each simulation (Figure 3b) confirms that the backbone of PM2 is the least solvated, while the backbone atoms of the unstapled peptide have the highest degree of solvation. Reduced backbone hydration has been observed to favor helicity in peptides[56]. Although PM2-PEG shows a lower degree of backbone hydration, the polar atoms of the hydrophilic PEG chain can form hydrogen bonds with the amide groups of the backbone, thus interfering with the intra-peptide hydrogen bonds that are needed to stabilize the helical conformations (Figures 4b, 4d).

3.2 How hydrocarbon stapling modulates binding to the receptor

Peptides are flexible molecules, and their conformations are very much dependent on their micro-environment, as we have seen in the section above. To understand how the micro-environment of the binding pocket affects the conformations of the four peptides, we performed a series of HREMD simulations for each of them in the presence of MDM2. For each peptide, we first explored the behavior of the peptide located in the canonical binding pocket of MDM2. Subsequently, the peptide was gradually moved away from the binding pocket. Along the chosen unbinding coordinate, each peptide was restrained to remain at distances of 1.4, 1.7 and 2.1 nm from MDM2, and at each distance, the systems were subjected to 300 ns HREMD simulations. Figure 5 shows the secondary structural evolution of the four peptides at different distances and Table S3 shows the corresponding percentages of helicity. In the bound state without any restraints, all peptides adopt higher populations of helical conformations compared to those in solution, and this is not surprising since the binding pocket of MDM2 provides the geometric constraints in which the peptide fluctuates around its helical conformation. It is clear that the hydrophobic character and the shape complementarity of the binding pocket favor helicity. The lack of the constraining chain in PM2-spring/PM2-linear enables them to adjust their conformations in the hydrophobic pocket, maximizing the intrahelical hydrogen bonds. In comparison the chains in PM2/PM2-PEG act as restraints that result in somewhat restricted adjustment and hence lesser helicities. Even at 1.4nm (the distance between the centre of mass of MDM2 and the peptides), the peptides are close to some of the MDM2 side chains, and the staples/PEG chains do interact with them (e.g., with Phe55, Gln61 etc). When the peptides are pulled a little away from the binding pocket, e.g., at the restraint distance of 1.4 nm, all the peptides still maintain high populations of helicity as they are still within the hydrophobic binding pocket (Figure S5). As the

peptide further moves away from the binding pocket, e.g., in the case of restrained distances of 1.7 nm, the peptide gradually loses its helicity. At the largest restrained distance of 2.1 nm, the peptides are completely out of the binding pocket, resulting in a significant reduction in the helicity of the peptide. Compared to the other three peptides, PM2 displays minimum reduction in helicity, from 57% in the binding pocket to 46% when it is out of the binding pocket (e.g., at restraint distance of 2.1 nm), followed by PM2-PEG whose helicity decreases from 58% to 24%. In contrast, the other two peptides show significant reduction in helicities (60% to 9% for PM2-linear and 62% to 9% for PM2-spring) due to the absence of the staple chain. This suggests that PM2 pays the least entropic penalty upon binding to MDM2. Although at 2.1 nm, the peptides are out of the binding pocket, the peptides still appear to experience the effects of MDM2, particularly through long-range electrostatic interactions. As a result, the structural properties of the peptides at 2.1 nm from MDM2 are not exactly the same as those in solution. For example, the helicities at 2.1 nm and in solution respectively are: 46% vs 38%; 9% vs 14%; 24% vs 17% and 9% vs 31% for PM2, PM2-linear, PM2-PEG and PM2-spring. The former three peptides show similar helicity between at 2.1 nm and in solution, while PM2-spring displays larger difference, suggesting that the interactions between peptide and MDM2 at 2.1 nm have more significant effect on PM2-spring. The number of hydration water molecules (Table S4) increases when the peptide moves out of the binding pocket to 2.1 nm, and further increases when the peptides are in bulk solvent; this is in general to be expected. Figure S6 shows that the pairwise RMSD distribution in solution is close to that at 2.1 nm except for PM2-spring, whose pairwise RMSD moves to larger value compared to that at 2.1 nm. The higher fluctuations of PM2-spring in solution compared to that at 2.1 nm suggests that PM2-spring experiences stronger interactions with MDM2 which restricts its conformational flexibility.

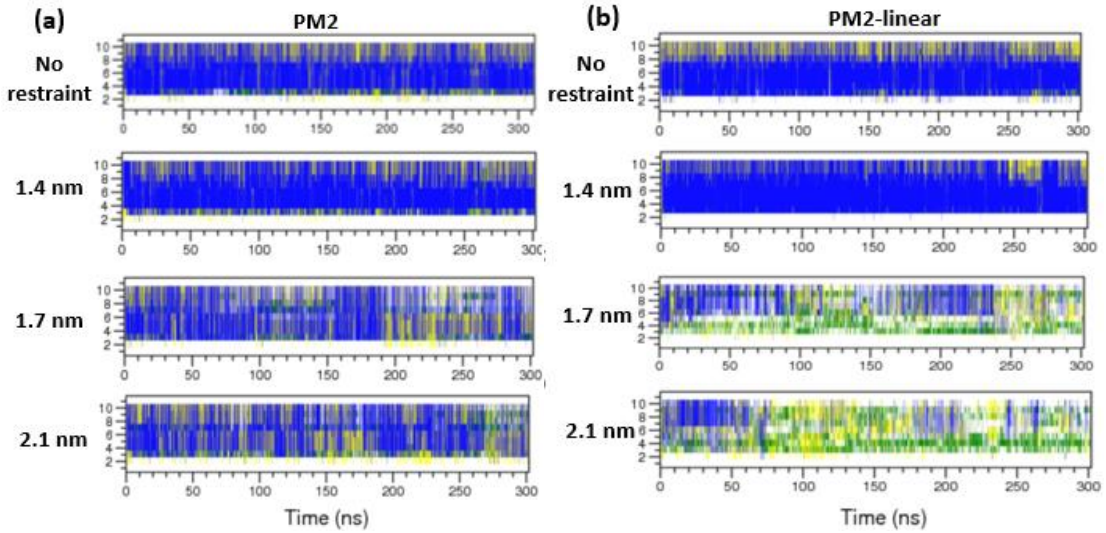

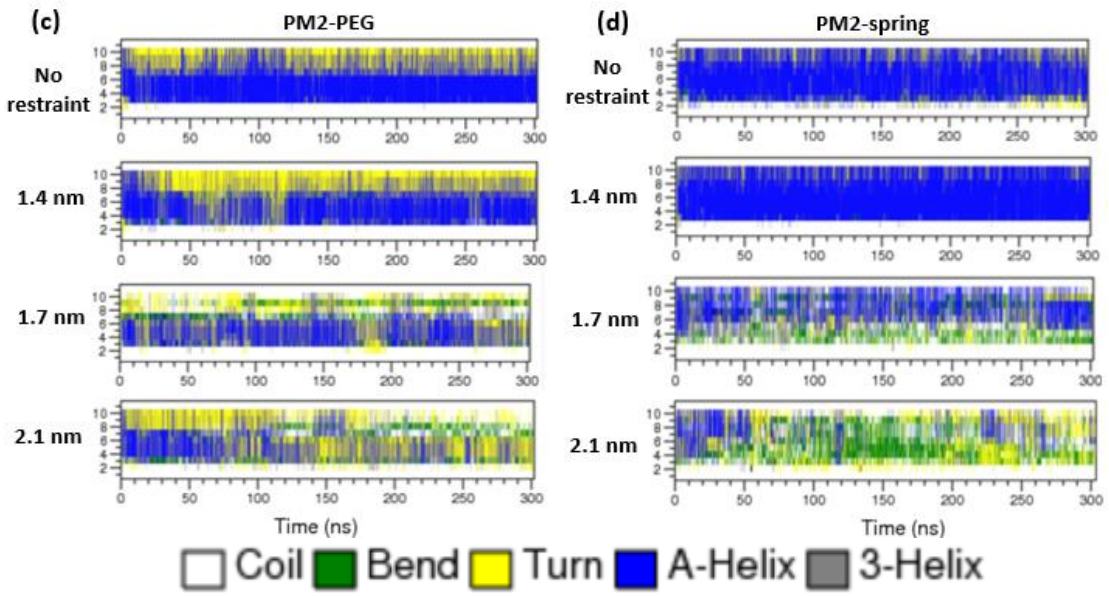

Figure 5. Secondary structure evolution of the four peptides at different restraint distances away from MDM2 during the last 200ns of the 300ns HREMD simulations

We next clustered the conformations of the peptide in each HREMD simulation and representative conformations of the complexes taken from the first cluster are shown in Figure S5. When the peptide is restrained at 1.7 nm, the two stapled peptides: PM2 and PM2-PEG are still partially inserted in the binding pocket, while the other two peptides PM2-linear and PM2-spring have already emerged out of the binding pocket (but still interact with MDM2). This suggests that the staple and the helical nature of the peptides is intimately coupled to the dynamics of the pocket of MDM2 which clearly is engaged in stabilizing interactions with these 2 peptides. At 2.1 nm, all the peptides are out of the binding pocket and the corresponding helicity is significantly reduced. Although the hydration of the peptide increases as the peptide moves out of the binding pocket (TableS4), the peptides restrained at 2.1 nm differ from free peptides in solution because at the restrained distance, the peptide still experiences interactions from MDM2, particularly the long-range electrostatic interactions. This can be seen from the smaller hydration number (e.g., number of water molecules with 0.5 nm of the peptide molecule) at 2.1 nm compared to the peptide in solution (Table S4). To further understand how the staple chain mediates the interactions with MDM2, we calculated the number of atomic contacts of MDM2 with the peptide and the staple chain, respectively (Figure S7). An atomic contact is defined if the distance of one heavy atom of the peptide and one heavy atom of MDM2 is within 0.5 nm. Then the ratio of the two numbers of atomic contacts can tell the orientation of the peptide with respect to MDM2. At restraint distance of 2.1 nm, the ratios for both PM2 and PM2-PEG peptides show a broad distribution, suggesting both peptides adopt various orientations with respect to MDM2. At the restraint distance of 1.7 nm where the peptide partially inserts into the MDM2, a high peak in the distribution appears at large ratio for PM2, while the peak shifts to lower ratio

when the PM2 further inserts into the binding pocket, suggesting that the initial atomic contacts are primarily mediated by the hydrocarbon staple chain of PM2. For the PM2-PEG peptide, at the restraint distance of 1.7 nm, the peak at large ratio decreases and an additional peak at very low ratio appears, suggesting that the atomic contacts between the PEG chain and MDM2 are not as stable as the hydrocarbon chain of PM2.

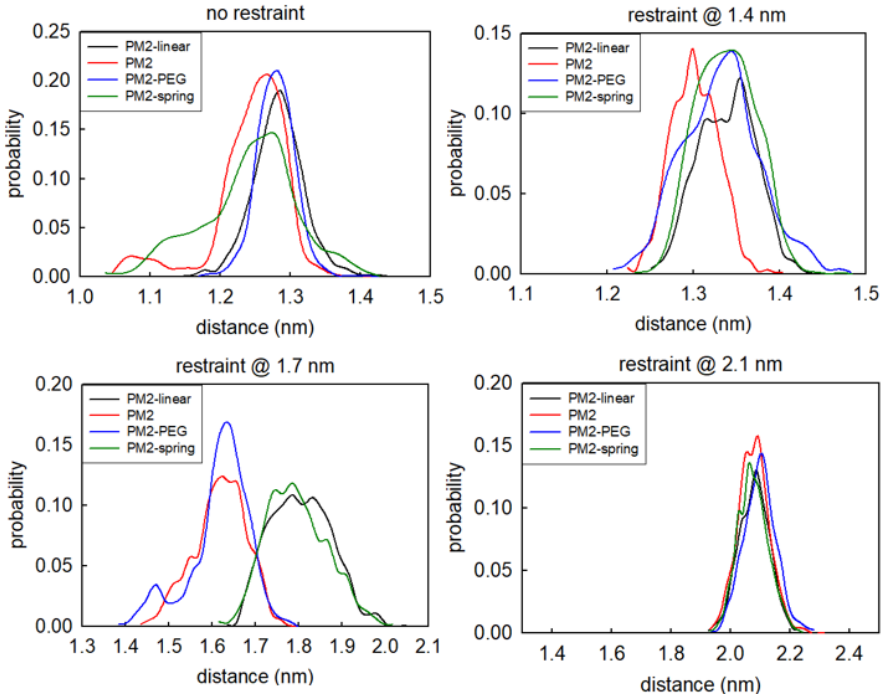

Figure 6. Distribution of the peptide MDM2 distances, with the peptide located at different distances from MDM2. The calculations were carried out over the last 200 ns of the simulations.

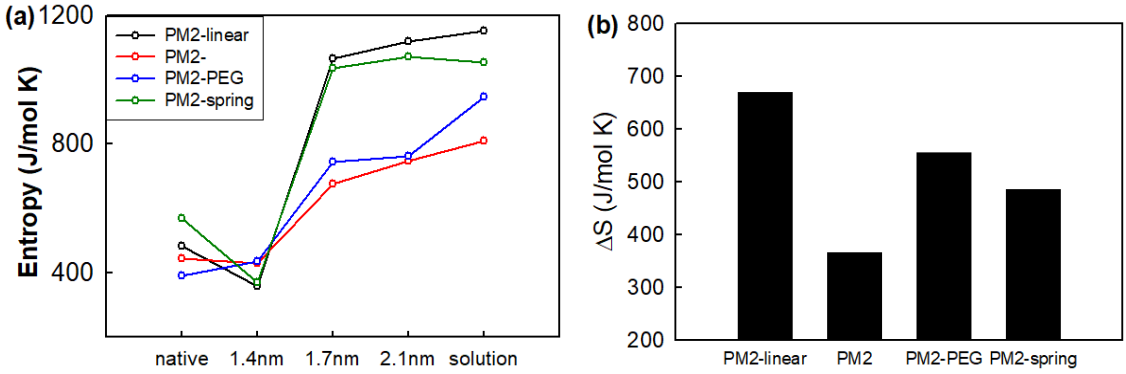

Figure 7. Configurational entropy of the four peptides in different states calculated using quasi-harmonic approximation (a) and the loss of configurational entropy between peptide in solution and in binding pocket of MDM2 (b).

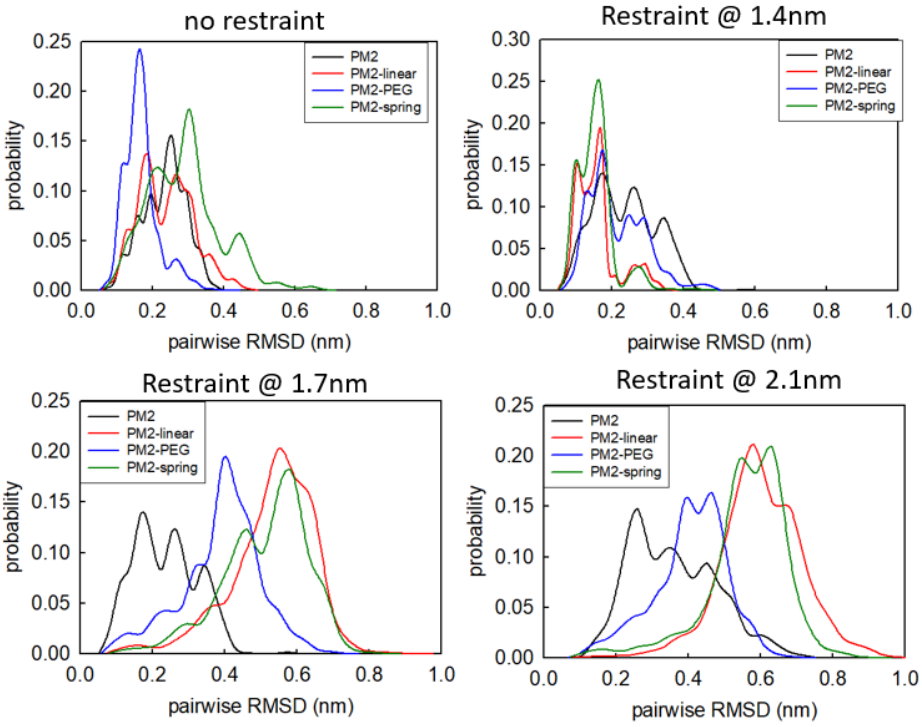

Figure8. Pairwise RMSD of the peptides in complex with MDM2, with the peptide located at different distances from MDM2. The calculations were carried out over the last 200 ns of the simulations.

Next, we explore the effect that stapling on the binding affinity of PM2 to MDM2. Peptide stapling has been shown to be an important contribution to the overall free energy of binding[32, 49, 50]. Due to the complex free energy surface of the peptide-MDM2 system, direct calculation of the binding free energy is challenging. However, an approximation may be made regarding the relative binding affinities by the extent of deviation of the peptides from the restrained distances (Figure 6). When the peptide is in the binding pocket without any restraints, all four peptides show similar distance distributions. At 1.4 nm, all peptides show distance distributions that are slightly smaller than 1.4 nm, suggesting that all peptides tend to rebind to MDM2. PM2 shows the shortest distance, indicating the highest tendency of rebinding to MDM2. As the restrained distance increases to 1.7 nm, the PM2 and PM2-PEG display shorter distances than 1.7 nm (the restrained distance), while PM2-spring and PM2-linear show larger distances than 1.7 nm. This results from the former two peptides remaining partially inserted in the binding pocket, while the latter two move out of the binding pocket (Figure S5). The contrasting distance distributions suggest that both hydrocarbon and the PEG staple chains contribute to the binding affinity, resulting in higher affinity for MDM2, which is consistent with previous computational observations showing that at small displacements away from the binding pocket, the stapled peptide has a higher probability of rebinding to the binding pocket than the PM2-linear peptides [42]. We further calculated the energetics of binding

of each peptide with MDM2 using the MMPBSA protocol implemented in GROMACS[94-96]. Table S5 shows that the two stapled peptides PM2 and PM2-PEG are more energetically favorable in binding to MDM2 than the two unstapled peptides PM2-linear and PM2-spring. The two stapled peptides essentially bind with similar affinities (given the large standard deviations). While the gas phase interactions between MDM2 and the peptides are in the order PM2 > PM2-linear > PM2-spring > PM2-PEG, however the PM2-PEG balances this with a favorable desolvation term; in contrast the rest of the peptides pay a penalty for desolvation as they are sequestered into MDM2 from solvent. The presence of the three polar atoms on the PEG chain imparts favorable solvation energy. It should be noted that the MMPBSA method has limitations which include the lack of entropic terms (some are captured by the solvation terms) and it employs an implicit solvent model, which cannot capture the water mediated binding. Advanced sampling methods such as thermodynamic integration (TI), in theory, can give more accurate results, but are largely limited to small molecules. Using TI to calculate the binding free energy of peptide to protein is still challenging due to insufficient sampling and convergence issue. Despite its limitations, the MMPBSA method provides a rapid method with reasonable accuracy and is an attractive approach to examine the energetics of peptide binding to protein[97].

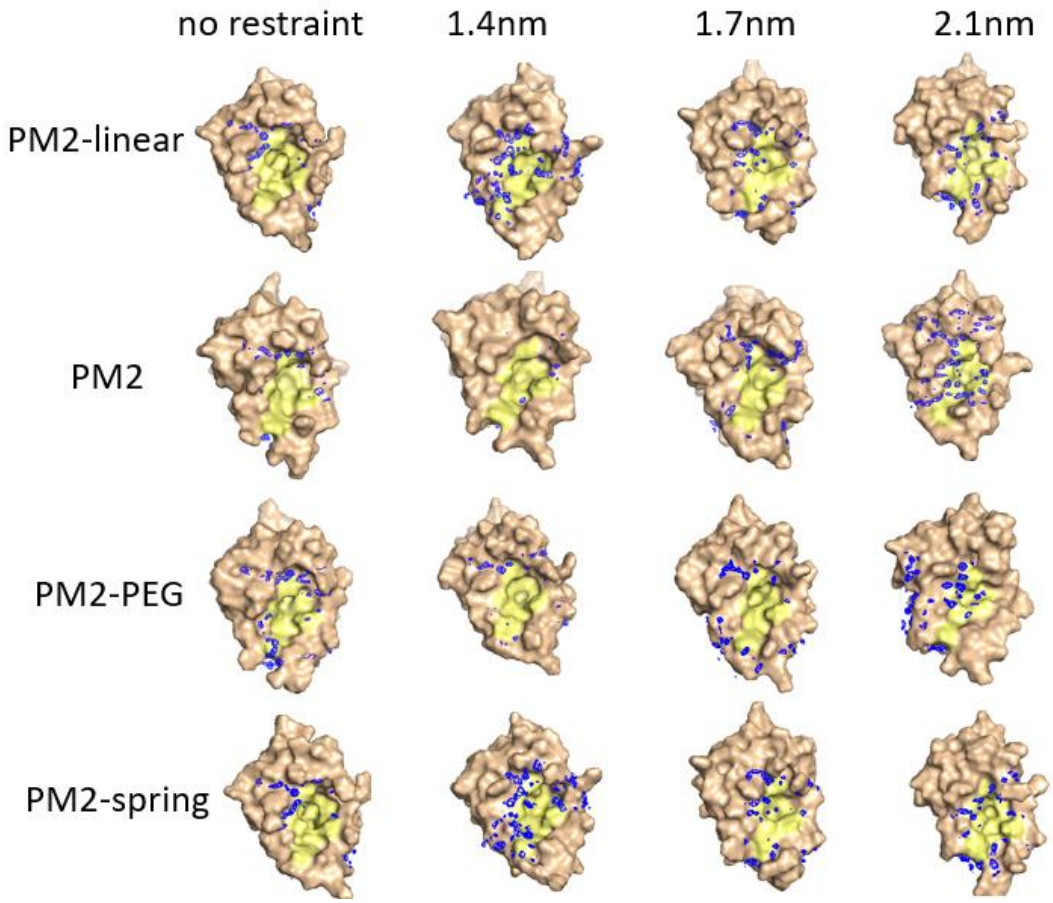

Figure 9. Grid based water density around the binding pocket of MDM2 with the peptide at different distances from MDM2. The water density (blue mesh) is calculated based on the last 200 ns of each simulation. The yellow surface denotes the binding pocket.

The conformational transition of the peptide along the pathway can also be seen by PCA analysis. Figures S8 shows that when the peptides are within or in the immediate vicinity of the binding pocket (no restraint or 1.4 nm), there are very few minima in the free energy landscape as the system is dominated by the interactions between MDM2 and the helical conformations. When the peptides gradually move out of the binding pocket, the free energy landscape becomes more frustrated, suggesting many more metastable conformational states. Unsurprisingly, PM2 experiences less perturbation to its helicity because of the constraints imposed by the staple chain. This suggests that clearly PM2 will pay a lower entropic cost than the PM2-linear peptide upon binding. The population shift along the pathway can also be seen from the percentage of the first cluster of each peptide (Figure S5). In the binding pocket, all peptides display high population of helical conformations, while out of the binding pocket, the population of the first cluster for PM2 is 31%, while it is much lower for all other peptides. Particularly the population of the 1st cluster for PM2-linear drops to 2.9%, suggesting that this peptide will incur a much higher entropic penalty upon binding to MDM2. To quantify the entropic loss of the

peptide during binding, we calculated the change of configurational entropy of the four peptides using quasi harmonic approximation (Figure 7). As expected, the PM2 has the lowest configurational entropy in solution. Although all the four peptides experience entropy loss when approaching the binding pocket, PM2 displays the lowest entropy loss upon binding.

To further understand the effect of binding on peptide conformation, we calculated the pairwise RMSD of each peptide. Figure 8 shows that in the binding pocket without restraints (no restrained potential) or under a small deviation from the binding pocket (e.g., at 1.4 nm), all peptides show small pairwise RMSD because they are largely helical. As the peptide moves out of the binding pocket (1.7 and 2.1 nm), the pairwise RMSD distribution shifts to much higher values, indicating that the peptides become more dynamic. Again, PM2 displays the smallest increase in the pairwise RMSD, followed by PM2-PEG. The results suggest that the conformational dynamics of the peptides are modulated by the interplay between the micro-environment and the staple chain.

We next explored the effects of the peptides on the solvation of the receptor. In the absence of the peptides, the binding pocket is solvated with water molecules. Peptide binding to MDM2 results in desolvation of the binding pocket, as has been demonstrated in previous computational studies[50, 98]. We calculated the grid-based water density around the binding pocket when the peptide is at different distances (Figure 9). We also calculated the number of water molecules in the binding pocket (Figure S9) which we define as the number of water molecules within 0.5 nm of a set of reference atoms of MDM2 (e.g., the heavy atoms in the sidechains of L57, I61 and I99, the CE1 atom of F91, the CD atom of I93 and the CD atom of I103). When the peptide is in the binding pocket, the binding pocket is desolvated and water molecules can only access the edge of the binding pocket, as a result of the excluded volume effect of the peptide molecule. When the peptide is at 1.4 nm, the peptides remain in the pocket and hence the binding pocket is still desolvated, especially for the two stapled peptides PM2 and PM2-PEG due to the excluded volume of their staple chain. In such a case, even though single water molecules may transiently penetrate into the space between the peptide and MDM2, that water molecule will not be able to engage in thermodynamically favorable interactions (hydrogen bonds) in the hydrophobic environment; this results in dewetting, a phenomena that was observed to occur between planar hydrophobic molecules (e.g., two graphene molecules) as well as between protein surfaces[99, 100]. In contrast, for PM2-linear and PM2-spring, the pockets are solvated to a greater extent because the lack of staple chain provides available volume to accommodate water molecules near the binding pocket. At larger distances between the peptides and MDM2 (1.7 nm), when there is sufficient space between the peptide and MDM2, solvation of the binding pocket starts. Although at distance of 1.7 nm, there are large space to accommodate water molecules between the peptide and MDM2, PM2 displays the lower degree of solvation, and the

solvation is mainly at the edge of the binding pocket. Figure S7 also suggests that at distance of 1.7 nm, the hydrocarbon chain of PM2 faces the binding pocket, suggesting hydrophobicity of the staple contribute to the desolvation of the binding pocket. At 2.1 nm, all peptides move out of the binding pocket, the binding pocket becomes fully solvated. Since the peptide-MDM2 binding interface is hydrophobic in nature, the increase in solvation of the binding pocket can also be seen from the reduction of hydrophobic solvent accessible surface area (SASA) of the binding pocket upon binding (Figure S10). When the peptide is in the binding pocket or at 1.4 nm, PM2 and PM2-PEG result in higher desolvation of the binding pocket, hence likely resulting in higher binding affinity.

4. Discussion

Stapled peptides are a promising new class of drug candidates being developed to target protein-protein interfaces. Their design is still fraught with complex issues and unknowns such as the determination of the optimal stapling sites, the chemistry of the stapled chain, the cell permeability etc. It is clear that hydrocarbon stapling may modulate the peptide conformation via constraint and hydrophobic effects. To understand the relative importance of these two factors, we chose a well characterized stapled peptide PM2, together with 3 modelled peptide variants of PM2 and explored their dynamics, solution conformations and interactions with MDM2. By modifying the hydrocarbon staple chain into a harmonic spring, we found that the constraint effect significantly reduces the conformational flexibility of the peptide and restricts the peptide from non-helical conformations. Replacement of the hydrocarbon staple chain with a hydrophilic PEG chain demonstrates that the hydrophobicity of the staple chain favors helical conformation of PM2 because the hydrocarbon chain can nucleate the hydrophobic residues to stabilize the helical conformation, a phenomenon similar to the cooperativity of the Zimm-Bragg or Lifson-Roig models in which the helicity of the peptide depends on the intrinsic helical propensity of individual residues as well as the cooperativity of the nearby residues [101, 102].

MD simulations of the complexes of these peptides with their receptor MDM2 revealed the added importance of the micro-environment in modulating the peptide conformations [56]. The binding pocket of MDM2 is characterized by a large and deep hydrophobic cavity that complements the shape of the four model peptides when they are in a helical conformation. Due to the shape of the binding pocket, the flexibilities of the four peptides are attenuated upon binding, particularly for PM2-linear and PM2-spring, which show low tendency to rebind MDM2 when they are in the vicinity of the binding pocket. PM2 exhibits the least extensive conformational change upon binding, followed by PM2-PEG, resulting in reduced entropic penalty upon binding[12, 13]. The other two peptides display

large population shifts in their conformational states upon binding. Moreover, the stapling chain also modulates the binding affinity by direct interactions with MDM2. Compared to the bound state, the structures of the unbound peptides in solution are very dynamic and display only small populations of helical conformations that are in equilibrium with non-helical conformations. When the helical conformations of the peptide are docked into the binding pocket to form a complex, the population of the helical conformations of the unbound peptide decreases in solution. As a result, more and more non-helical conformations are transformed to helical conformations, driven by the thermodynamic equilibrium between helical and non-helical conformations of the unbound peptide. Therefore, binding of the peptide to MDM2 can be viewed as a two-step process with two thermodynamic equilibria: the equilibrium between helical conformations and non-helical conformations of the unbound peptide; the equilibrium between helical conformations of the unbound peptide and the helical conformations of the peptide in the binding pocket. PM2 displays a high population of helical conformations in solution, therefore the binding can be approximated as a one-step process that only involves an equilibrium between helical conformations of unbound PM2 and helical conformations of PM2 in the binding pocket; this results in higher binding affinity for MDM2. In contrast, binding of the other three peptides seems to depend on the interplay of the two equilibria at least. Moreover, the hydrocarbon staple chain also favors dehydration of the hydrophobic surface of the binding pocket of MDM2, further contributing to the binding affinity. And finally the hydrocarbon staple contributes to the binding by engaging in direct interactions with the surface residues of MDM2, as has been shown previously too [32, 49, 50, 103].

The findings of this study suggest some guidelines towards the design of staple peptides. Firstly, to maintain helical conformation, the staple chain should not interfere with the hydrogen bonds between backbone atoms. Secondly, stabilization of the side chain of the peptides can be used to stabilize the helical conformation, as evidenced by the hydrophobic interactions of the hydrocarbon staple chain with the Phe and Trp residues of PM2. For example, if the peptide contains positively charged residues, one may consider incorporating aromatic moieties to engage cation-pi interactions. Thirdly, to enhance binding, one can engineer direct interactions between the staple chain and the receptor. For instance, if the binding pocket of the receptor is hydrophilic in nature, one can incorporate polar groups in the staple, such as in the form of PEG-staples[104] to engage favorable interactions with the receptor. Finally, stapling may also affect other pharmaceutical properties of the peptides such as membrane permeability and solubility. It has been shown that stapling enhances the membrane permeability of some peptides[7, 19] because (i) it increases the overall hydrophobicity (ii) enhances the helical conformations such that the polar backbone atoms not only are buried inside, but also form intramolecular hydrogen bonds, resulting in less desolvation free energy when the peptide transits to the membrane phase. In addition, hydrocarbon stapling may lower the peptide

solubility. To overcome this, several stapling strategies (e.g., triazole stapling) have been used to enhance the solubility of the stapled peptide[105, 106]. Clearly there will be additional developments that will catalyze the progress of this class of molecules as effective probes of protein-protein interactions and as therapeutics.

Supporting Information

Sequence of the peptides, percentage of helicity and hydration number of the peptides, snapshots of the peptide in solution and in complex with the receptor, free energy landscape of the peptides and other associated figures.

Acknowledgements

The authors would like to thank BMRC/A*STAR ACRC and NSCC for providing the computational resources.

Conflict of Interest

CSV is the founder of SiNOPSEE Therapeutics and Aplomex; this work has no conflict with the companies.

References

Uncategorized References

1. Henninot, A.; Collins, J. C.; Nuss, J. M. The Current State of Peptide Drug Discovery: Back to the Future? *Journal of Medicinal Chemistry* **2018,** 61, 1382-1414.
2. Lau, J. L.; Dunn, M. K. Therapeutic peptides: Historical perspectives, current development trends, and future directions. *Bioorganic & Medicinal Chemistry* **2018,** 26, 2700-2707.
3. Di, L. Strategic Approaches to Optimizing Peptide ADME Properties. *The AAPS Journal* **2015,** 17, 134-143.
4. Lau, Y. H.; de Andrade, P.; Wu, Y.; Spring, D. R. Peptide stapling techniques based on different macrocyclisation chemistries. *Chemical Society Reviews* **2015,** 44, 91-102.
5. Hillman, R. A.; Nadraws, J. W.; Bertucci, M. A. The Hydrocarbon Staple & Beyond: Recent Advances Towards Stapled Peptide Therapeutics that Target Protein-protein Interactions. *Current Topics in Medicinal Chemistry* **2018,** 18, 611-624.
6. Bluntzer, M. T. J.; O'Connell, J.; Baker, T. S.; Michel, J.; Hulme, A. N. Designing stapled peptides to inhibit protein-protein interactions: An analysis of successes in a rapidly changing field. *Peptide Science* **2021,** 113, e24191.
7. Paterson, D. L.; Flanagan, J. U.; Shepherd, P. R.; Harris, P. W. R.; Brimble, M. A. Variable-Length Ester-Based Staples for α-Helical Peptides by Using A Double Thiol-ene Reaction. *Chemistry-A European Journal* **2020,** 26, 10826-10833.
8. Lai, Y.; Fois, G.; Flores, J. R.; Tuvim, M. J.; Zhou, Q.; Yang, K.; Leitz, J.; Peters, J.; Zhang, Y.; Pfuetzner, R. A.; Esquivies, L.; Jones, P.; Frick, M.; Dickey, B. F.; Brunger, A. T. Inhibition of calcium-triggered secretion by hydrocarbon-stapled peptides. *Nature* **2022,** 603, 949-956.

9. Choudhury, A. R.; Maity, A.; Chakraborty, S.; Chakrabarti, R. Computational design of stapled peptide inhibitor against SARS-CoV-2 receptor binding domain. *Peptide Science* **2022,** 114, e24267.
10. Calugi, L.; Sautariello, G.; Lenci, E.; Mattei, M. L.; Coppa, C.; Cini, N.; Contini, A.; Trabocchi, A. Identification of a short ACE2-derived stapled peptide targeting the SARS-CoV-2 spike protein. *European Journal of Medicinal Chemistry* **2023,** 249, 115118.
11. Schnorenberg, M. R.; Hawley, K. M.; Thomas-Toth, A. T.; Watkins, E. A.; Tian, Y.; Ting, J. M.; Leak, L. B.; Kucera, I. M.; Raczy, M. M.; Kung, A. L.; Hubbell, J. A.; Tirrell, M. V.; LaBelle, J. L. Targeted Polymersome Delivery of a Stapled Peptide for Drugging the Tumor Protein p53:BCL-2-Family Axis in Diffuse Large B-Cell Lymphoma. *ACS Nano* **2023**.
12. Unarta, I. C.; Xu, J.; Shang, Y.; Cheung, C. H. P.; Zhu, R.; Chen, X.; Cao, S.; Cheung, P. P.-H.; Bierer, D.; Zhang, M.; Huang, X.; Li, X. Entropy of stapled peptide inhibitors in free state is the major contributor to the improvement of binding affinity with the GK domain. *RSC Chemical Biology* **2021,** 2, 1274-1284.
13. Maity, A.; Choudhury, A. R.; Chakrabarti, R. Effect of Stapling on the Thermodynamics of mdm2–p53 Binding. *Journal of Chemical Information and Modeling* **2021,** 61, 1989-2000.
14. Marqusee, S.; Baldwin, R. L. Helix stabilization by Glu-...Lys+ salt bridges in short peptides of de novo design. *Proc Natl Acad Sci U S A* **1987,** 84, 8898-8902.
15. Meuzelaar, H.; Vreede, J.; Woutersen, S. Influence of Glu/Arg, Asp/Arg, and Glu/Lys Salt Bridges on α-Helical Stability and Folding Kinetics. *Biophysical Journal* **2016,** 110, 2328-2341.
16. Sommese, R. F.; Sivaramakrishnan, S.; Baldwin, R. L.; Spudich, J. A. Helicity of short E-R/K peptides. *Protein Sci* **2010,** 19, 2001-2005.
17. Jain, A.; Verma, R. K.; Sankararamakrishnan, R. Presence of Intra-helical Salt-Bridge in Loop E Half-Helix Can Influence the Transport Properties of AQP1 and GlpF Channels: Molecular Dynamics Simulations of In Silico Mutants. *J Membr Biol.* **2019,** 252, 17-29.
18. Walensky, L. D.; Bird, G. H. Hydrocarbon-Stapled Peptides: Principles, Practice, and Progress. *Journal of Medicinal Chemistry* **2014,** 57, 6275-6288.
19. Sun, T.-L.; Sun, Y.; Lee, C.-C.; Huang, H. W. Membrane permeability of hydrocarbon-cross-linked peptides. *Biophysical journal* **2013,** 104, 1923-1932.
20. Cromm, P. M.; Spiegel, J.; Grossmann, T. N. Hydrocarbon Stapled Peptides as Modulators of Biological Function. *ACS Chemical Biology* **2015,** 10, 1362-1375.
21. Cornillie, S. P.; Bruno, B. J.; Lim, C. S.; Cheatham, T. E., III. Computational Modeling of Stapled Peptides toward a Treatment Strategy for CML and Broader Implications in the Design of Lengthy Peptide Therapeutics. *The Journal of Physical Chemistry B* **2018,** 122, 3864-3875.
22. Choudhury, A. R.; Maity, A.; Chakraborty, S.; Chakrabarti, R. Computational design of stapled peptide inhibitor against SARS-CoV-2 receptor binding domain. **2022,** 114, e24267.
23. Speltz, T. E.; Fanning, S. W.; Mayne, C. G.; Fowler, C.; Tajkhorshid, E.; Greene, G. L.; Moore, T. W. Stapled Peptides with γ-Methylated Hydrocarbon Chains for the Estrogen Receptor/Coactivator Interaction. *Angewandte Chemie International Edition* **2016,** 55, 4252-4255.
24. Adak, A.; Das, G.; Gupta, V.; Khan, J.; Mukherjee, N.; Mondal, P.; Roy, R.; Barman, S.; Gharai, P. K.; Ghosh, S. Evolution of Potential Antimitotic Stapled Peptides from Multiple Helical Peptide Stretches of the Tubulin Heterodimer Interface: Helix-Mimicking Stapled Peptide Tubulin Inhibitors. *Journal of Medicinal Chemistry* **2022,** 65, 13866-13878.
25. Schafmeister, C. E.; Po, J.; Verdine, G. L. An All-Hydrocarbon Cross-Linking System for Enhancing the Helicity and Metabolic Stability of Peptides. *Journal of the American Chemical Society* **2000,** 122, 5891-5892.

26. Bird, G. H.; Madani, N.; Perry, A. F.; Princiotto, A. M.; Supko, J. G.; He, X.; Gavathiotis, E.; Sodroski, J. G.; Walensky, L. D. Hydrocarbon double-stapling remedies the proteolytic instability of a lengthy peptide therapeutic. *Proceedings of the National Academy of Sciences* **2010,** 107, 14093-14098.
27. Lau, Y. H.; de Andrade, P.; Quah, S.-T.; Rossmann, M.; Laraia, L.; Sköld, N.; Sum, T. J.; Rowling, P. J. E.; Joseph, T. L.; Verma, C.; Hyvönen, M.; Itzhaki, L. S.; Venkitaraman, A. R.; Brown, C. J.; Lane, D. P.; Spring, D. R. Functionalised staple linkages for modulating the cellular activity of stapled peptides. *Chemical Science* **2014,** 5, 1804-1809.
28. Dietrich, L.; Rathmer, B.; Ewan, K.; Bange, T.; Heinrichs, S.; Dale, T. C.; Schade, D.; Grossmann, T. N. Cell Permeable Stapled Peptide Inhibitor of Wnt Signaling that Targets β-Catenin Protein-Protein Interactions. *Cell Chemical Biology* **2017,** 24, 958-968.e5.
29. Verdine, G. L.; Hilinski, G. J. All-hydrocarbon stapled peptides as Synthetic Cell-Accessible Mini-Proteins. *Drug Discovery Today: Technologies* **2012,** 9, e41-e47.
30. Chu, Q.; Moellering, R. E.; Hilinski, G. J.; Kim, Y.-W.; Grossmann, T. N.; Yeh, J. T. H.; Verdine, G. L. Towards understanding cell penetration by stapled peptides. *MedChemComm* **2015,** 6, 111-119.
31. Verdine, G. L.; Hilinski, G. J. Chapter one - Stapled Peptides for Intracellular Drug Targets. In *Methods in Enzymology*, Wittrup, K. D.; Verdine, G. L., Eds. Academic Press: 2012; Vol. 503, pp 3-33.
32. Baek, S.; Kutchukian, P. S.; Verdine, G. L.; Huber, R.; Holak, T. A.; Lee, K. W.; Popowicz, G. M. Structure of the Stapled p53 Peptide Bound to Mdm2. *Journal of the American Chemical Society* **2012,** 134, 103-106.
33. Bird, G. H.; Boyapalle, S.; Wong, T.; Opoku-Nsiah, K.; Bedi, R.; Crannell, W. C.; Perry, A. F.; Nguyen, H.; Sampayo, V.; Devareddy, A.; Mohapatra, S.; Mohapatra, S. S.; Walensky, L. D. Mucosal delivery of a double-stapled RSV peptide prevents nasopulmonary infection. *The Journal of clinical investigation* **2014,** 124, 2113-24.
34. Rezaei Araghi, R.; Bird, G. H.; Ryan, J. A.; Jenson, J. M.; Godes, M.; Pritz, J. R.; Grant, R. A.; Letai, A.; Walensky, L. D.; Keating, A. E. Iterative optimization yields Mcl-1-targeting stapled peptides with selective cytotoxicity to Mcl-1-dependent cancer cells. *Proc Natl Acad Sci U S A* **2018,** 115, E886-e895.
35. Mourtada, R.; Herce, H. D.; Yin, D. J.; Moroco, J. A.; Wales, T. E.; Engen, J. R.; Walensky, L. D. Design of stapled antimicrobial peptides that are stable, nontoxic and kill antibiotic-resistant bacteria in mice. *Nature Biotechnology* **2019,** 37, 1186-1197.
36. Bird, G. H.; Irimia, A.; Ofek, G.; Kwong, P. D.; Wilson, I. A.; Walensky, L. D. Stapled HIV-1 peptides recapitulate antigenic structures and engage broadly neutralizing antibodies. *Nature structural & molecular biology* **2014,** 21, 1058-67.
37. Guerlavais, V.; Sawyer, T. K.; Carvajal, L.; Chang, Y. S.; Graves, B.; Ren, J.-G.; Sutton, D.; Olson, K. A.; Packman, K.; Darlak, K.; Elkin, C.; Feyfant, E.; Kesavan, K.; Gangurde, P.; Vassilev, L. T.; Nash, H. M.; Vukovic, V.; Aivado, M.; Annis, D. A. Discovery of Sulanemadlin (ALRN-6924), the First Cell-Permeating, Stabilized α-Helical Peptide in Clinical Development. *Journal of Medicinal Chemistry* **2023,** 66, 9401-9417.
38. Kannan, S.; Aronica, P. G. A.; Ng, S.; Gek Lian, D. T.; Frosi, Y.; Chee, S.; Shimin, J.; Yuen, T. Y.; Sadruddin, A.; Kaan, H. Y. K.; Chandramohan, A.; Wong, J. H.; Tan, Y. S.; Chang, Z. W.; Ferrer-Gago, F. J.; Arumugam, P.; Han, Y.; Chen, S.; Rénia, L.; Brown, C. J.; Johannes, C. W.; Henry, B.; Lane, D. P.; Sawyer, T. K.; Verma, C. S.; Partridge, A. W. Macrocyclization of an all-d linear α-helical peptide imparts cellular permeability. *Chemical Science* **2020,** 11, 5577-5591.

39. Cong, W.; Shen, H.; Liao, X.; Zheng, M.; Kong, X.; Wang, Z.; Chen, S.; Li, Y.; Hu, H.; Li, X. Discovery of an orally effective double-stapled peptide for reducing ovariectomy-induced bone loss in mice. *Acta Pharmaceutica Sinica B* **2023,** 13, 3770-3781.
40. Selvarajan, V.; Tram, N. D. T.; Xu, J.; Ngen, S. T. Y.; Koh, J.-J.; Teo, J. W. P.; Yuen, T.-Y.; Ee, P. L. R. Stapled β-Hairpin Antimicrobial Peptides with Improved Stability and Activity against Drug-Resistant Gram-Negative Bacteria. *Journal of Medicinal Chemistry* **2023,** 66, 8498-8509.
41. Ali, A. M.; Atmaj, J.; Van Oosterwijk, N.; Groves, M. R.; Dömling, A. Stapled Peptides Inhibitors: A New Window for Target Drug Discovery. *Comput Struct Biotechnol J* **2019,** 17, 263-281.
42. Sim, A. Y. L.; Verma, C. How does a hydrocarbon staple affect peptide hydrophobicity? *Journal of Computational Chemistry* **2015,** 36, 773-784.
43. Sim, A. Y. L.; Joseph, T.; Lane, D. P.; Verma, C. Mechanism of Stapled Peptide Binding to MDM2: Possible Consequences for Peptide Design. *Journal of Chemical Theory and Computation* **2014,** 10, 1753-1761.
44. Ovchinnikov, V.; Munasinghe, A.; Karplus, M. Molecular Simulation of Stapled Peptides. In *Computational Peptide Science: Methods and Protocols*, Simonson, T., Ed. Springer US: New York, NY, 2022; pp 283-301.
45. Bernal, F.; Tyler, A. F.; Korsmeyer, S. J.; Walensky, L. D.; Verdine, G. L. Reactivation of the p53 tumor suppressor pathway by a stapled p53 peptide. *Journal of the American Chemical Society* **2007,** 129, 2456-2457.
46. Robert, A. H.; Jonathan, W. N.; Michael, A. B. The Hydrocarbon Staple & Beyond: Recent Advances Towards Stapled Peptide Therapeutics that Target Protein-Protein Interactions. *Current Topics in Medicinal Chemistry* **2018,** 18, 611-624.
47. Guerlavais, V.; Sawyer, T. K. Chapter Twenty-One - Advancements in Stapled Peptide Drug Discovery & Development. In *Annual Reports in Medicinal Chemistry*, Desai, M. C., Ed. Academic Press: 2014; Vol. 49, pp 331-345.
48. Guo, Z.; Mohanty, U.; Noehre, J.; Sawyer, T. K.; Sherman, W.; Krilov, G. Probing the α-Helical Structural Stability of Stapled p53 Peptides: Molecular Dynamics Simulations and Analysis. *Chemical Biology & Drug Design* **2010,** 75, 348-359.
49. Joseph, T. L.; Lane, D.; Verma, C. S. Stapled peptides in the p53 pathway: Computer simulations reveal novel interactions of the staples with the target protein. *Cell Cycle* **2010,** 9, 4560-4568.
50. Guo, Z.; Streu, K.; Krilov, G.; Mohanty, U. Probing the Origin of Structural Stability of Single and Double Stapled p53 Peptide Analogs Bound to MDM2. *Chemical Biology & Drug Design* **2014,** 83, 631-642.
51. Morrone, J. A.; Perez, A.; Deng, Q.; Ha, S. N.; Holloway, M. K.; Sawyer, T. K.; Sherborne, B. S.; Brown, F. K.; Dill, K. A. Molecular Simulations Identify Binding Poses and Approximate Affinities of Stapled α-Helical Peptides to MDM2 and MDMX. *Journal of Chemical Theory and Computation* **2017,** 13, 863-869.
52. Wallraven, K.; Holmelin, F. L.; Glas, A.; Hennig, S.; Frolov, A. I.; Grossmann, T. N. Adapting free energy perturbation simulations for large macrocyclic ligands: how to dissect contributions from direct binding and free ligand flexibility. *Chemical Science* **2020,** 11, 2269-2276.
53. Coffill, C. R.; Lee, A. P.; Siau, J. W.; Chee, S. M.; Joseph, T. L.; Tan, Y. S.; Madhumalar, A.; Tay, B.-H.; Brenner, S.; Verma, C. S.; Ghadessy, F. J.; Venkatesh, B.; Lane, D. P. The p53–Mdm2 interaction and the E3 ligase activity of Mdm2/Mdm4 are conserved from lampreys to humans. *Genes & Development* **2016,** 30, 281-292.

54. Chandler, D. Interfaces and the driving force of hydrophobic assembly. *Nature* **2005,** 437, 640-647.
55. Lee, X. A.; Verma, C.; Sim, A. Y. L. Designing dual inhibitors of Mdm2/MdmX: Unexpected coupling of water with gatekeeper Y100/99. *Proteins: Structure, Function, and Bioinformatics* **2017,** 85, 1493-1506.
56. Li, J.; Hu, Z.; Beuerman, R.; Verma, C. Molecular Environment Modulates Conformational Differences between Crystal and Solution States of Human β-Defensin 2. *The Journal of Physical Chemistry B* **2017,** 121, 2739-2747.
57. Brown, C. J.; Quah, S. T.; Jong, J.; Goh, A. M.; Chiam, P. C.; Khoo, K. H.; Choong, M. L.; Lee, M. A.; Yurlova, L.; Zolghadr, K.; Joseph, T. L.; Verma, C. S.; Lane, D. P. Stapled Peptides with Improved Potency and Specificity That Activate p53. *ACS Chemical Biology* **2013,** 8, 506-512.
58. Chee, S. M. Q.; Wongsantichon, J.; Soo Tng, Q.; Robinson, R.; Joseph, T. L.; Verma, C.; Lane, D. P.; Brown, C. J.; Ghadessy, F. J. Structure of a Stapled Peptide Antagonist Bound to Nutlin-Resistant Mdm2. *PLOS ONE* **2014,** 9, e104914.
59. Pazgier, M.; Liu, M.; Zou, G.; Yuan, W.; Li, C.; Li, C.; Li, J.; Monbo, J.; Zella, D.; Tarasov, S. G.; Lu, W. Structural basis for high-affinity peptide inhibition of p53 interactions with MDM2 and MDMX. *Proceedings of the National Academy of Sciences* **2009,** 106, 4665-4670.
60. Chee, S. M. Q.; Wongsantichon, J.; Siau, J.; Thean, D.; Ferrer, F.; Robinson, R. C.; Lane, D. P.; Brown, C. J.; Ghadessy, F. J. Structure-activity studies of Mdm2/Mdm4-binding stapled peptides comprising non-natural amino acids. *PLOS ONE* **2017,** 12, e0189379.
61. Spiegelberg, D.; Mortensen, A. C.; Lundsten, S.; Brown, C. J.; Lane, D. P.; Nestor, M. The MDM2/MDMX-p53 Antagonist PM2 Radiosensitizes Wild-Type p53 Tumors. *Cancer Research* **2018,** 78, 5084-5093.
62. Wang, L.; Friesner, R. A.; Berne, B. J. Replica Exchange with Solute Scaling: A More Efficient Version of Replica Exchange with Solute Tempering (REST2). *The Journal of Physical Chemistry B* **2011,** 115, 9431-9438.
63. Liu, P.; Kim, B.; Friesner, R. A.; Berne, B. J. Replica exchange with solute tempering: A method for sampling biological systems in explicit water. *PNAS* **2005,** 102, 13749-13754.
64. Bussi, G. Hamiltonian replica exchange in GROMACS: a flexible implementation. *Molecular Physics* **2014,** 112, 379-384.
65. Ostermeir, K.; Zacharias, M. Advanced replica-exchange sampling to study the flexibility and plasticity of peptides and proteins. *Biochimica et Biophysica Acta (BBA) - Proteins and Proteomics* **2013,** 1834, 847-853.
66. Terakawa, T.; Kameda, T.; Takada, S. On easy implementation of a variant of the replica exchange with solute tempering in GROMACS. *Journal of Computational Chemistry* **2011,** 32, 1228-1234.
67. Stephen John, F.; Jianguo, L.; Yaw Sing, T.; Minh, N. N.; Arumay, P.; Zohra, O.; Shilpa, Y.; Srinivasaraghavan, K. The Multifaceted Roles of Molecular Dynamics Simulations in Drug Discovery. *Current Pharmaceutical Design* **2016,** 22, 3585-3600.
68. Sugita, Y.; Okamoto, Y. Replica-exchange molecular dynamics method for protein folding. *Chemical Physics Letters* **1999,** 314, 141-151.
69. Smith, A. K.; Lockhart, C.; Klimov, D. K. Does Replica Exchange with Solute Tempering Efficiently Sample Aβ Peptide Conformational Ensembles? *Journal of Chemical Theory and Computation* **2016,** 12, 5201-5214.
70. Hornak, V.; Abel, R.; Okur, A.; Strockbine, B.; Roitberg, A.; Simmerling, C. Comparison of multiple Amber force fields and development of improved protein backbone parameters. *Proteins: Structure, Function, and Bioinformatics* **2006,** 65, 712-725.

71. Jorgensen, W. L.; Chandrasekhar, J.; Madura, J. D.; Impey, R. W.; Klein, M. L. Comparison of simple potential functions for simulating liquid water. *The Journal of Chemical Physics* **1983,** 79, 926-935.
72. Lee, X. A.; Verma, C.; Sim, A. Y. L. Designing dual inhibitors of Mdm2/MdmX: Unexpected coupling of water with gatekeeper Y100/99. **2017,** 85, 1493-1506.
73. Sim, A. Y. L.; Verma, C. How does a hydrocarbon staple affect peptide hydrophobicity? **2015,** 36, 773-784.
74. Wickstrom, L.; Okur, A.; Simmerling, C. Evaluating the Performance of the ff99SB Force Field Based on NMR Scalar Coupling Data. *Biophysical Journal* **2009,** 97, 853-856.
75. Cerutti, D. S.; Freddolino, P. L.; Duke, R. E., Jr.; Case, D. A. Simulations of a Protein Crystal with a High Resolution X-ray Structure: Evaluation of Force Fields and Water Models. *The Journal of Physical Chemistry B* **2010,** 114, 12811-12824.
76. Maier, J. A.; Martinez, C.; Kasavajhala, K.; Wickstrom, L.; Hauser, K. E.; Simmerling, C. ff14SB: Improving the Accuracy of Protein Side Chain and Backbone Parameters from ff99SB. *Journal of Chemical Theory and Computation* **2015,** 11, 3696-3713.
77. Pantelopulos, G. A.; Mukherjee, S.; Voelz, V. A. Microsecond simulations of mdm2 and its complex with p53 yield insight into force field accuracy and conformational dynamics. *Proteins* **2015,** 83, 1665-76.
78. Wang, J.; Wang, W.; Kollman, P. A.; Case, D. A. Automatic atom type and bond type perception in molecular mechanical calculations. *Journal of Molecular Graphics and Modelling* **2006,** 25, 247-260.
79. Essmann, U.; Perera, L.; Berkowitz, M. L.; Darden, T.; Lee, H.; Pedersen, L. G. A smooth particle mesh Ewald method. *The Journal of Chemical Physics* **1995,** 103, 8577-8593.
80. Kabsch, W.; Sander, C. Dictionary of protein secondary structure: Pattern recognition of hydrogen-bonded and geometrical features. *Biopolymers* **1983,** 22, 2577-2637.
81. D.A. Case. et al. AMBER 2020. *University of California, San Francisco* **2020**.
82. Hou, T.; Wang, J.; Li, Y.; Wang, W. Assessing the Performance of the MM/PBSA and MM/GBSA Methods. 1. The Accuracy of Binding Free Energy Calculations Based on Molecular Dynamics Simulations. *Journal of Chemical Information and Modeling* **2011,** 51, 69-82.
83. Kar, P.; Lipowsky, R.; Knecht, V. Importance of polar solvation and configurational entropy for design of antiretroviral drugs targeting HIV-1 protease. *The journal of physical chemistry. B* **2013,** 117, 5793-805.
84. Bjelkmar, P.; Larsson, P.; Cuendet, M. A.; Hess, B.; Lindahl, E. Implementation of the CHARMM Force Field in GROMACS: Analysis of Protein Stability Effects from Correction Maps, Virtual Interaction Sites, and Water Models. *Journal of Chemical Theory and Computation* **2010,** 6, 459-466.
85. Bonomi, M.; Branduardi, D.; Bussi, G.; Camilloni, C.; Provasi, D.; Raiteri, P.; Donadio, D.; Marinelli, F.; Pietrucci, F.; Broglia, R. A.; Parrinello, M. PLUMED: A portable plugin for free-energy calculations with molecular dynamics. *Computer Physics Communications* **2009,** 180, 1961-1972.
86. Armen, R.; Alonso, D. O.; Daggett, V. The role of alpha-, 3(10)-, and pi-helix in helix-->coil transitions. *Protein Sci* **2003,** 12, 1145-57.
87. Millhauser, G. L. Views of helical peptides: a proposal for the position of 3(10)-helix along the thermodynamic folding pathway. *Biochemistry* **1995,** 34, 3873-7.
88. Armen, R.; Alonso, D. O. V.; Daggett, V. The role of alpha-, 3(10)-, and pi-helix in helix-->coil transitions. *Protein Sci* **2003,** 12, 1145-1157.
89. Dike, A.; Cowsik, S. M. Solution structure of amphibian tachykinin Uperolein bound to DPC micelles. *Journal of Structural Biology* **2006,** 156, 442-452.

90. Chipot, C.; Pohorille, A. Folding and Translocation of the Undecamer of Poly-l-leucine across the Water−Hexane Interface. A Molecular Dynamics Study. *Journal of the American Chemical Society* **1998,** 120, 11912-11924.
91. Kuzmanic, A.; Zagrovic, B. Determination of ensemble-average pairwise root mean-square deviation from experimental B-factors. *Biophysical journal* **2010,** 98, 861-871.
92. Fox, S. J.; Lakshminarayanan, R.; Beuerman, R. W.; Li, J.; Verma, C. S. Conformational Transitions of Melittin between Aqueous and Lipid Phases: Comparison of Simulations with Experiments. *The Journal of Physical Chemistry B* **2018,** 122, 8698-8705.
93. Roccatano, D.; Colombo, G.; Fioroni, M.; Mark, A. E. Mechanism by which 2,2,2-trifluoroethanol/water mixtures stabilize secondary-structure formation in peptides: A molecular dynamics study. *Proceedings of the National Academy of Sciences* **2002,** 99, 12179-12184.
94. Kumari, R.; Kumar, R.; Lynn, A. g_mmpbsa—A GROMACS Tool for High-Throughput MM-PBSA Calculations. *Journal of Chemical Information and Modeling* **2014,** 54, 1951-1962.
95. Wang, E.; Sun, H.; Wang, J.; Wang, Z.; Liu, H.; Zhang, J. Z. H.; Hou, T. End-Point Binding Free Energy Calculation with MM/PBSA and MM/GBSA: Strategies and Applications in Drug Design. *Chemical Reviews* **2019,** 119, 9478-9508.
96. Sun, H.; Duan, L.; Chen, F.; Liu, H.; Wang, Z.; Pan, P.; Zhu, F.; Zhang, J. Z. H.; Hou, T. Assessing the performance of MM/PBSA and MM/GBSA methods. 7. Entropy effects on the performance of end-point binding free energy calculation approaches. *Physical Chemistry Chemical Physics* **2018,** 20, 14450-14460.
97. Weng, G.; Wang, E.; Chen, F.; Sun, H.; Wang, Z.; Hou, T. Assessing the performance of MM/PBSA and MM/GBSA methods. 9. Prediction reliability of binding affinities and binding poses for protein-peptide complexes. *Physical chemistry chemical physics : PCCP* **2019,** 21, 10135-10145.
98. Guo, Z.; Li, B.; Dzubiella, J.; Cheng, L.-T.; McCammon, J. A.; Che, J. Heterogeneous Hydration of p53/MDM2 Complex. *Journal of chemical theory and computation* **2014,** 10, 1302-1313.
99. Hua, L.; Zangi, R.; Berne, B. J. Hydrophobic Interactions and Dewetting between Plates with Hydrophobic and Hydrophilic Domains. *The Journal of Physical Chemistry C* **2009,** 113, 5244-5253.
100. Liu, P.; Huang, X.; Zhou, R.; Berne, B. J. Observation of a dewetting transition in the collapse of the melittin tetramer. *Nature* **2005,** 437, 159-162.
101. Lifson, S.; Roig, A. On the Theory of Helix—Coil Transition in Polypeptides. *Journal of Chemical Physics* **1961,** 34, 1963-1974.
102. Zimm, B. H.; Bragg, J. K. Theory of the Phase Transition between Helix and Random Coil in Polypeptide Chains. *Journal of Chemical Physics* **1959,** 31, 526-535.
103. Im, H.; Ham, S. Effect of linker on the binding free energy of stapled p53/HDM2 complex. *PloS one* **2020,** 15, e0232613-e0232613.
104. Xiao, Q.; Ashton, D. S.; Jones, Z. B.; Thompson, K. P.; Price, J. L. Long-range PEG stapling: macrocyclization for increased protein conformational stability and resistance to proteolysis. *RSC Chemical Biology* **2020,** 1, 273-280.
105. Smeenk, L. E. J.; Dailly, N.; Hiemstra, H.; van Maarseveen, J. H.; Timmerman, P. Synthesis of Water-Soluble Scaffolds for Peptide Cyclization, Labeling, and Ligation. *Organic Letters* **2012,** 14, 1194-1197.
106. Kawamoto, S. A.; Coleska, A.; Ran, X.; Yi, H.; Yang, C.-Y.; Wang, S. Design of Triazole-Stapled BCL9 α-Helical Peptides to Target the β-Catenin/B-Cell CLL/lymphoma 9 (BCL9) Protein–Protein Interaction. *Journal of Medicinal Chemistry* **2012,** 55, 1137-1146.